Journal of Solid State Chemistry 181 (2008) 1930–1935

Contents lists available at ScienceDirect

Journal of Solid State Chemistry

journal homepage: www.elsevier.com/locate/jssc

Raman, XRD and microscopic investigations on CeO_2–Lu_2O_3 and CeO_2–Sc_2O_3 systems: A sub-solidus phase evolution study

V. Grover [a], Ankita Banerji [b], P. Sengupta [c], A.K. Tyagi [a,*]

[a] Chemistry Division, Bhabha Atomic Research Centre, Mumbai-400 085, India
[b] High Pressure Physics Division, Bhabha Atomic Research Centre, Mumbai-400 085, India
[c] Material Science Division, Bhabha Atomic Research Centre, Mumbai-400 085, India

ARTICLE INFO

Article history:
Received 21 November 2007
Received in revised form
25 March 2008
Accepted 3 April 2008
Available online 11 April 2008

Keywords:
Rare-earths oxides
XRD
Raman spectroscopy
Phase relations

ABSTRACT

A sub-solidus phase evolution study was done in CeO_2–Sc_2O_3 and CeO_2–Lu_2O_3 systems under slow-cooled conditions from 1400 °C. Long-range order probing of X-ray diffraction technique is utilized in conjunction with the ability of Raman spectroscopy to detect the changes in local co-ordination. Lu_2O_3 showed solubility of 30 mol% in CeO_2, thus forming an anion deficient fluorite-type (F-type) solid solution, whereas Sc_2O_3 did not show any discernible solubility. A biphasic region (F+C) was unequivocally detected by Raman spectroscopy in $Ce_{1-x}Lu_xO_{2-x/2}$ ($0.4 \leqslant x \leqslant 0.9$) and in $Ce_{1-x}Sc_xO_{2-x/2}$ ($0.1 \leqslant x \leqslant 0.9$) systems. Raman spectroscopy was valuable in studying these systems since oxygen vacancies are created on doping RE_2O_3 into ceria and Raman spectroscopy is very much sensitive to oxygen polarizability and local coordination. Back scattered images collected on representative compositions support the above-mentioned results.

1. Introduction

Ceria, doped with rare-earth (RE) oxides, is an important material in view of applications in oxygen concentration cells and in solid oxide fuel cells [1,2]. CeO_2 forms solid solution with oxides of different RE elements over a wide range of composition [3,4]. When a Ce^{4+} cationic sublattice of CeO_2 structure gets substituted with a trivalent RE ion, oxygen vacancies are created in anionic sublattice [1,5], which increases oxygen diffusion within the host lattice and drastically affects oxygen uptake and release by the system. The accompanying phase changes are also very interesting.

Pure ceria has fluorite (F-type) structure (space group $Fm\bar{3}m$). The structure of RE sesquioxides as a function of temperature and as well as ionic size has been lucidly elaborated upon by Adachi and Imanaka [6] in their review article on binary RE oxides. At normal temperature and pressure conditions, trivalent RE oxides ($MO_{1.5}$) crystallize in three general structure types, namely hexagonal (A), monoclinic (B) or cubic (C), depending on the ionic radii of the RE ions (6). The A-type RE_2O_3 exists for RE = La to Nd. In general, on going from La to Lu, the structure of RE_2O_3 changes from A-type to B-type to C-type. The heavier RE oxides (with smaller cationic radius), like Lu_2O_3 retain the C-type form well upto 2000 °C. The C-form is of the cubic bixbyite [$(Fe, Mn)_2O_3$] type (space group Ia-3) containing 32 metal atoms and 48 oxygen atoms per unit cell. The metal atoms are six-coordinated. In the F-type cubic structure of dioxide (CeO_2), the metal atom is eight co-ordinated with cubic co-ordination polyhedra sharing all edges to form a three-dimensional network. If one-fourth oxygens are removed along the nonintersecting strings in the four $\langle 111 \rangle$ directions, then all metal ions will have a six-fold co-ordination resulting in a C-type structure. Thus, the C-type structure is closely related to the fluorite lattice in a way of the ordered vacancy in fluorite lattice ($a_{\text{C-type}} = 2 \times a_{\text{Fluorite}}$).

In RE doped ceria, lattice parameters and other physical properties of the samples tend to change with composition and are an interesting interplay of relative sizes of Ce^{4+} and RE^{3+} as well as the oxygen vacancies created as the result of this aliovalent substitution [7]. Also, this may lead to the stabilization of high temperature phases of REs at ambient temperature. This makes the study of phase evolution in RE doped ceria an interesting research area. Since the aliovalent substitution of RE^{3+} into CeO_2 results in the generation of oxygen vacancies, it would be interesting to see the effect of oxygen vacancies on the phase evolution. However, X-ray diffraction (XRD) technique is found to be insensitive to microscopic phase changes initiated by oxygen displacement, because X-ray scattering efficiency of oxygen is significantly lower as compared to that of the high Z RE cations. Moreover, owing to large coherence length of X-rays, it is not often easy to detect parasitic micro domains of altogether different new

* Corresponding author. Fax: +91 22 2550 5050/+91 22 2551 9613.
E-mail address: aktyagi@barc.ernet.in (A.K. Tyagi).

0022-4596/$ - see front matter © 2008 Elsevier Inc. All rights reserved.
doi:10.1016/j.jssc.2008.04.001

phases amidst a bulk phase using XRD technique [8]. Raman spectroscopy becomes useful in such cases and promises better results because of its sensitivity to both oxygen displacement due to large polarizability [9] and intermediate range order without long range periodicity [2,10]. In particular, the Raman spectrum of the perfect crystal lattice undergoes drastic changes in the presence of any disorder in the system and proves to be an excellent probe for local disorder. Secondly, oxygen vibrations rising from the dopant can be studied separately from those of the host cations by Raman spectroscopy.

In this particular study, XRD technique, which is more sensitive to disorder in the cationic sublattice compared to anionic sublattice, has been utilized in conjunction with Raman spectroscopy, which is primarily sensitive to oxygen-cation vibrations, and provides both short as well as long range ordering to study the phase evolution in CeO_2–Sc_2O_3 and CeO_2–Lu_2O_3 systems. Also, since Lu^{3+} (0.88 Å) and Sc^{3+} (0.77 Å) have quite different ionic radii, it would be of interest to examine the effect of size on phase evolution in these two systems, despite the similar structure of RE_2O_3 (C-type).

2. Experimental

CeO_2, Sc_2O_3 and Lu_2O_3 (all 99.9%) were used as the starting materials, which were heated at 900 °C for overnight prior to the further use. These starting materials were well characterized by powder XRD before use. About 20 nominal compositions in CeO_2–Sc_2O_3 and CeO_2–Lu_2O_3 system were prepared by a three-stage heating protocol, as follows: the intimately ground mixtures were heated in the pellet form at 1200 °C for 36 h, followed by second heating at 1300 °C for 36 h after regrinding and repelletizing. In order to attain a better homogeneity, the products obtained after second heating were reground, pelletized and heated at 1400 °C for 48 h, which was the final annealing temperature of all the specimens. The heating and cooling rates were 2°/min in all the annealing steps and atmosphere was static air. The starting materials and all the nominal compositions prepared were characterized by powder XRD. The XRD patterns were recorded on a Philips X-ray diffractometer (Model PW 1710) with monochromatized Cu-$K\alpha$ radiation. Silicon was used as an external standard for calibration of the instrument. The XRD patterns were analyzed by comparing with the reported ones. In order to determine the solubility limits, the lattice parameters were refined by the least squares method.

The Raman spectra were excited using 532 nm line from a solid state laser. The scattered light over the range 100–1700 cm^{-1} was analyzed using a single stage 0.9 m spectrograph (with notch filter) and back thinned CCD detector.

Samples for back scattered electron imaging were polished to 1 μm diamond finish by conventional metallographic techniques. The samples were coated with thin gold layer ($\approx$10 nm) for ensuring conductivity. In order to acquire high contrast for back scattered electron images, the acceleration voltage was generally kept in the range of 25–30 keV and the beam current around 1–4 nA.

3. Results and discussion

3.1. $Ce_{1-x}Lu_xO_{2-x/2}$

The XRD patterns of all the products in $Ce_{1-x}Lu_xO_{2-x/2}$ series were recorded and analyzed. The parent compounds CeO_2 is fluorite-type cubic ($Fm\bar{3}m$), whereas Lu_2O_3 is C-type cubic (Ia-3). C-type cubic structure is a superstructure of fluorite-type structure. The evolution of the phase relation for this particular series is shown in Fig. 1. It was observed that on doping 10 mol% $LuO_{1.5}$ into CeO_2, the XRD pattern consisted of peaks due to fluorite-type lattice. This implies that 10 mol% Lu_2O_3 is soluble in CeO_2, and hence this nominal composition is monophasic fluorite-type. On increasing the concentration of Lu_2O_3 to 30 mol%, the pattern still consisted of peaks due to F-type phase only. The fluorite-type peaks were found to shift towards higher angle with increase in amount of Lu_2O_3 thereby further indicating the solubility of Lu_2O_3 into CeO_2. The ionic radius of Lu^{3+} is smaller than Ce^{4+} [11], which is manifested in the decrease in lattice parameter. Beyond that, i.e. on doping 40 mol% Lu_2O_3, peaks corresponding to Lu_2O_3 appeared. Hence, the nominal composition $Ce_{0.6}Lu_{0.4}O_{1.8}$ is biphasic consisting of both F-type and C-type phases. On further increasing the concentration of $LuO_{1.5}$, the biphasicity is retained with concomitant increase in intensity of peaks corresponding to C-type phase and decrease in those representing F-type phase. This trend was continued till 90 mol% $LuO_{1.5}$. The lattice parameter of the F-type solid solution was found to decrease till the nominal composition $Ce_{0.6}Lu_{0.4}O_{1.8}$ and then it became constant from the onset of biphasic region onwards. The lattice parameter of the C-type phase was constant throughout. An important implication of this result is that lutetia lattice has no solubility of ceria in it, i.e. Lu_2O_3 is soluble in CeO_2, but vice versa is not observed. Foex and Traverse [12] have reported that the stability of C-type modification increases on decreasing the RE^{3+} ionic size from La^{3+} to Lu^{3+}. In fact, Lu_2O_3, which is C-type, does not undergo any phase transition as it directly melts. Probably this extra stability of C-type modification prevents the formation of anion excess C-type solid solution in Lu_2O_3 unlike the studies reported previously, wherein a monophasic C-type phase field ($RE_{1-y}Ce_yO_{1.5+y/2}$) was observed in $Ce_{1-x}RE_xO_{2-x/2}$ in RE_2O_3 rich region [7,10]. The ionic radius of Ce4+ is 0.90 Å and that of Lu^{3+} is 0.88 Å (both in 8-fold coordination). This shows that even though Lu^{3+} is smaller, their ionic sizes are not very different. Even then the lattice parameters show quite a significant reduction on doping Lu^{3+} ions. For every two RE^{3+} doped into the ceria lattice, one oxygen vacancy is created which also contributes to the lattice parameter trend. Thus the sharp decrease in lattice parameter can be explained on the basis of cumulative effect of oxygen vacancies, and the change

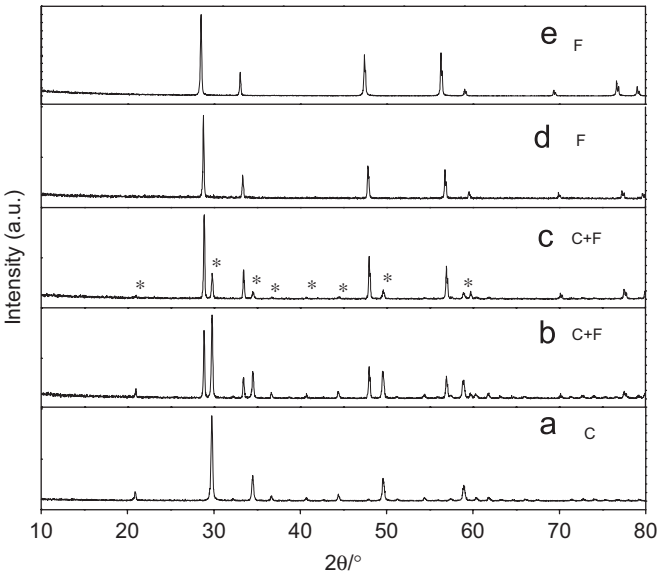

Fig. 1. Typical XRD patterns in $Ce_{1-x}Lu_xO_{2-x/2}$ series: (a) Lu_2O_3, (b) $Ce_{0.3}Lu_{0.7}O_{1.65}$, (c) $Ce_{0.5}Lu_{0.5}O_{1.75}$, (d) $Ce_{0.7}Lu_{0.3}O_{1.85}$ and (e) CeO_2.

in ionic radii and in this particular case it is mainly due to the effect of vacancies (since the size difference is not appreciable).

Fig. 2 shows a back scattered image of $Ce_{0.1}Lu_{0.9}O_{1.55}$. The bright spots belong to higher c phase (C-type phase), grey spots correspond to the lower Z phase (F-type) and black color are the pores. It is quite clear that the grey phase is very small in amount in accordance with the XRD result that the nominal composition, $Ce_{0.1}Lu_{0.9}O_{1.55}$, contains a majority of Lu-rich C-type phase and a minority of Ce-rich F-type phase.

Raman studies were also performed on the $Ce_{1-x}Lu_xO_{2-x/2}$ system. Cerium dioxide, CeO_2, crystallizes in the cubic fluorite-type lattice and belongs to the space group O_h^5 ($Fm3m$). Group theoretical analysis predicts only one triply degenerate Raman active optical phonon with F_{2g} symmetry which can be viewed as symmetric breathing mode of the oxygen atoms around each cation, and two infrared active phonons of F_{1u} symmetry corresponding to the LO and TO modes. Since only the O atoms move, the mode frequency should be nearly independent of the cation mass. The first order Raman spectrum of CeO_2 is very simple and consists of only one Raman mode at 465 cm^{-1}. The compounds having C-type structure, like Lu_2O_3, crystallize in the body centered lattice and belong to the space group $Ia3$ (T_h^7). The unit cell contains the two primitive cells having eight formula units. Factor group analysis of Lu_2O_3 predicts a total of 22 Raman active modes distributed as 4Ag+4Eg+14Fg. The ambient Raman spectrum and the different mode frequencies of both F-type CeO_2 and C-type Lu_2O_3 were recorded, and they agree quite well with the values reported in the literature [13,14]. All the allowed modes could not be observed in Lu_2O_3 except for the strongest mode at $\approx$390 cm^{-1} with some very weak peaks because of the low intensity and poor signal to noise ratio.

Fig. 3 shows the changes in the Raman spectra with increasing concentration of $LuO_{1.5}$ in CeO_2 over the frequency range 100–800 cm^{-1}. At 10 mol% $LuO_{1.5}$ doping, the Raman spectrum has a profile similar to F-type CeO_2. These similarities are indicative of the retention of the F-type phase up to 10 mol% Lu^{3+} substitution. No other changes in the Raman spectrum were observed except for the broadening of the F-type characteristic mode of CeO_2 at $\approx$465 cm^{-1}. Raman modes characteristic to pure Lu_2O_3 (C-type phase) are not observed in the nominal composition containing 10 mol% Lu^{3+} indicating that Lu^{3+} statistically replaces Ce^{4+} in the fluorite matrix. Such aliovalent replacements

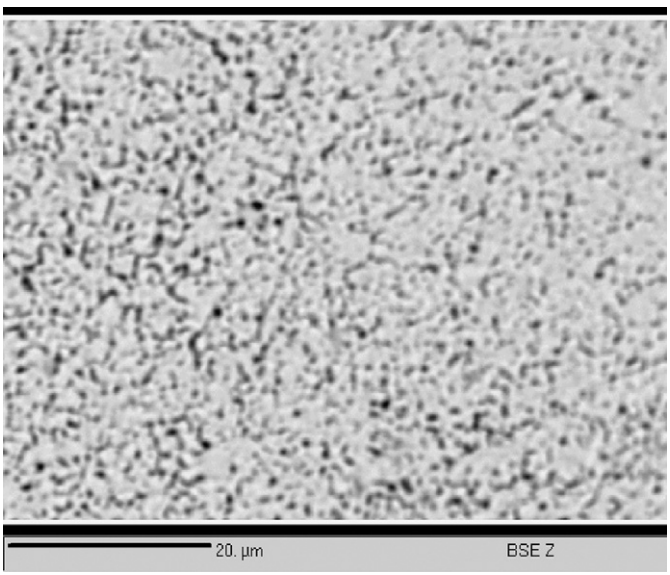

Fig. 2. Back scattered image of nominal composition $Ce_{0.1}Lu_{0.9}O_{1.55}$.

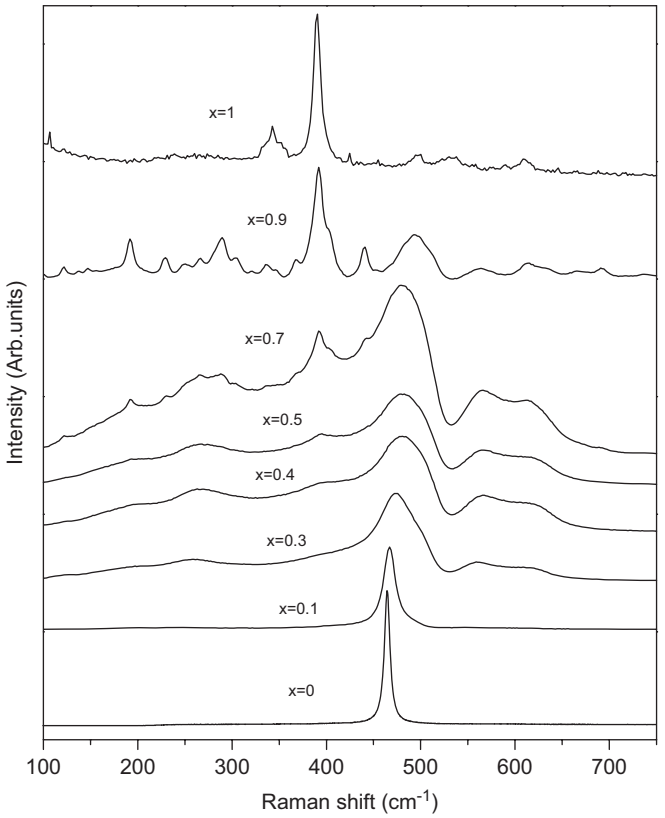

Fig. 3. Raman spectra from $Ce_{1-x}Lu_xO_{2-x/2}$ solid solution for values of x shown in the figure. Spectra have been vertically displaced for better clarity.

are accompanied by the creation of charge compensating vacancies on the anion sites [15]. At 40 mol% $LuO_{1.5}$, in addition to the characteristic F-type Raman mode at $\approx$465 cm^{-1} the Raman spectrum consists of broad features at $\approx$260, 562 and 609 cm^{-1}. The relative intensity of these broad modes increases as the Lu^{3+} content increases. It can be explained as in doped CeO_2, Ce^{4+} ions are partly replaced by the dopant cations (Lu^{3+}) at random introducing O^{2-} vacancies in the anionic sublattice. It is well known that Raman signal is affected by these randomly oriented vacancies that may distort long range ordering. The defect formation is a known source of structural disorder, and thus breakdown of translational symmetry occurs which results in relaxation of the $k\approx0$ selection rule for Raman scattering and hence phonons from all parts of the Brillouin zone contribute to the spectra. This explains the broadening of characteristic Raman mode of CeO_2 at 465 cm^{-1} and appearance of the new broad peaks with increase in the Lu^{3+} content. The origin of the broad modes could also be ascribed to the disorder induced scattering from different types of metal-oxygen-vacancy complexes [16]. In addition, we observe a distinct high frequency component at $\approx$490 cm^{-1} as a shoulder to the 465 cm^{-1} mode, which is again due to the disorder in fluorite-type lattice due to the doped Lu^{3+}. As we move to 40 mol% Lu^{3+} in CeO_2, the striking observation is the appearance of a broad mode centered at $\approx$390 cm^{-1} which is a characteristic C-type Raman mode. As the $LuO_{1.5}$ content increases, the width of this mode at $\approx$390 cm^{-1} decreases and its intensity increases, as against the intense mode of fluorite-type phase at 465 cm^{-1}, indicating the increase in amount of C-type phase. Also the intensity of the fluorite peak at 465 cm^{-1} further decreases and that of the other modes increases. For 70 mol% Lu^{3+} concentration, the characteristic peak of C-type at $\approx$390 cm^{-1} further sharpens, and when the Lu^{3+} concentration increases to

90 mol%, it appears with very strong intensity and the intensity of the characteristic peak of F-type structure diminishes considerably. This indicates that the biphasic region exists from 40 to 90 mol% Lu^{3+}. Another noteworthy observation was the blue shift of the frequency of the F-type mode at 465 cm^{-1} with increase in Lu^{3+} content from 10 to 40 mol% (Fig. 4) after which it attains a constant value till 90 mol% Lu^{3+}. The blue shift is observed due to the contraction of F-type lattice (Table 1) when Lu^{3+} substitutes for Ce^{4+}. On entering the biphasic region, the composition of F-type phase becomes constant and extra $LuO_{1.5}$ added thereafter gets separated as pure Lu_2O_3. This is manifested as near constancy in Raman frequency of the major F-type mode and C-type mode (due to Lu_2O_3). Also, it would be appropriate to mention here that XRD shows the onset of biphasicity from 40 mol% $LuO_{1.5}$ onwards which is also supported by constant decrease of lattice parameters up to 40 mol% $LuO_{1.5}$ and thereafter constancy of lattice parameter in the biphasic regime. The result was also corroborated by Raman spectroscopic studies, wherein the intense mode of Lu_2O_3 started becoming visible at 40 mol% $LuO_{1.5}$. However, if we observe very carefully, slight broadening is visible even at 30 mol% $LuO_{1.5}$ in the Raman spectrum though it is very subtle. It can be explained based on presence of C-type domains at a very small length scale in $Ce_{0.7}Lu_{0.3}O_{1.85}$ nominal composition which are not yet very prominent to give its signature, and hence to address it as a separate phase or not remains a question. Thus the Raman spectrum can be explained assuming that the solid solution $Ce_{1-x}Lu_xO_{2-x/2}$ exists as monophasic F-type solid solution for $x<0.4$ and as a biphasic region consisting of both the F- and C-type structures for $0.4 \leqslant x \leqslant 0.9$.

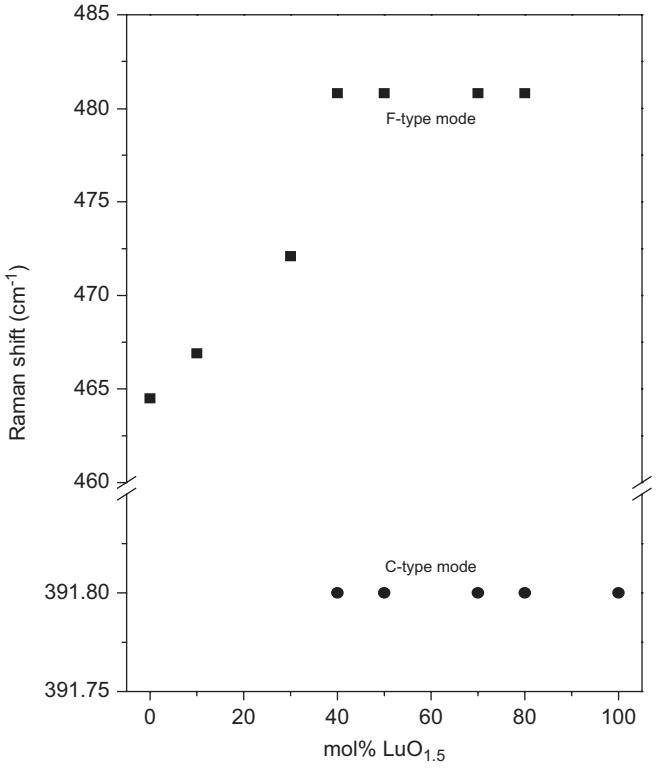

Fig. 4. Variation in peak frequency of the different Raman modes with increasing concentration of Lu.

Table 1
Phase analysis and room temperature lattice parameters of the phases in $Ce_{1-x}Lu_xO_{2-x/2}$ system, annealed at 1400 °C (in air) followed by slow cooling

S. no.	Nominal composition	Phase analyses	a(F) (Å)	a(C) (Å)
1	CeO_2	F	5.411(1)	–
2	$Ce_{0.90}Lu_{0.10}O_{1.95}$	F	5.410(1)	–
4	$Ce_{0.70}Lu_{0.30}O_{1.85}$	F	5.375(2)	–
5	$Ce_{0.60}Lu_{0.40}O_{1.80}$	F+C	5.361(2)	10.39(3)
6	$Ce_{0.50}Lu_{0.50}O_{1.75}$	F+C	5.360(1)	10.40(1)
8	$Ce_{0.30}Lu_{0.70}O_{1.65}$	F+C	5.361(1)	10.39(2)
10	$Ce_{0.10}Lu_{0.90}O_{1.55}$	F+C	5.361(1)	10.39(1)
11	Lu_2O_3	C	–	10.39(2)

3.2. $Ce_{1-x}Sc_xO_{2-x/2}$

The XRD patterns of all the products in $Ce_{1-x}Sc_xO_{2-x/2}$ series were recorded and analyzed. Sc_2O_3, like Lu_2O_3, is C-type cubic (*Ia*-3). It was observed that on doping 10 mol% CeO_2 into $ScO_{1.5}$, the XRD pattern consisted of peaks due to both Sc_2O_3 and CeO_2. This implies that even 10 mol% of ceria does not solubilize into Sc_2O_3 lattice. On doping 20 mol% CeO_2 into Sc_2O_3, the pattern still consisted of both Sc_2O_3 and ceria type peaks with concomitant increase in intensity of CeO_2-type peaks. The trend was continued in rest of the compositions, wherein the peaks due to CeO_2 increased in intensity with increase in ceria amount. Thus, the $Ce_{1-x}Sc_xO_{2-x/2}$ series is found to be biphasic throughout with F-type phase and C-type phase unlike $Ce_{1-x}Lu_xO_{2-x/2}$ series, wherein significant solubility of $LuO_{1.5}$ was observed in ceria lattice. However, on carefully examining the refined lattice parameters of fluorite-type solid solutions in different nominal compositions, it was observed that, on moving from pure ceria to $Ce_{0.9}Sc_{0.1}O_{1.95}$, there is a small but discernible decrease in the lattice parameter of ceria-type phase, which then became constant at that value (Table 2). This implies that a small amount of scandia has solubilized into ceria lattice, but this amount is evidently less than 10 mol%. The ionic radius of Ce^{4+} is 0.90 Å and Sc^{3+} is 0.75 Å (in 8-fold co-ordination) [11]. Hence, the small decrease of ionic radius can be explained on the basis of incorporation of smaller cation (Sc^{3+}) in place of larger cation (Ce^{4+}) in F-type lattice, thus indicating the solubility of small amount of scandia into ceria. Also, no variation was observed in the lattice parameter of C-type phase thus implying that there is no solubility of CeO_2 into scandia which appears plausible, because Ce^{4+} is a much bigger in size than Sc^{3+} as is illustrated by their ionic radii mentioned above. In fact, many studies have been done on CeO_2–RE_2O_3 systems, wherein ionic radii have been found to affect homogeneity region size as well as distribution of phase fields. For example, CeO_2–Nd_2O_3 has been studied by Pieczulewski et al. [17], wherein they have reported 37 mol% solubility of $NdO_{1.5}$ in CeO_2. Similar work has also been done by our group on CeO_2–RE_2O_3 (*RE*: Eu, Gd, Dy, Ho, Er, Tm, Yb)

Table 2
Phase analysis and room temperature lattice parameters of the phases in $Ce_{1-x}Sc_xO_{2-x/2}$ system, annealed at 1400 °C (in air) followed by slow cooling

S. no.	Nominal composition	Phase analyses	a(F) (Å)	a(C) (Å)
1	CeO_2	F	5.411(1)	
2	$Ce_{0.90}Sc_{0.10}O_{1.95}$	F+C	5.403(1)	[a]
3	$Ce_{0.80}Sc_{0.20}O_{1.90}$	F+C	5.405(1)	9.82(5)
4	$Ce_{0.70}Sc_{0.30}O_{1.85}$	F+C	5.404(1)	9.83(2)
5	$Ce_{0.60}Sc_{0.40}O_{1.80}$	F+C	5.404(1)	9.83(2)
6	$Ce_{0.50}Sc_{0.50}O_{1.75}$	F+C	5.404(2)	9.83(2)
7	$Ce_{0.40}Sc_{0.60}O_{1.70}$	F+C	5.405(1)	9.83(2)
8	$Ce_{0.30}Sc_{0.70}O_{1.65}$	F+C	5.406(2)	9.83(2)
9	$Ce_{0.20}Sc_{0.80}O_{1.60}$	F+C	5.405(1)	9.83(1)
10	$Ce_{0.10}Sc_{0.90}O_{1.55}$	F+C	5.405(1)	9.83(2)
11	Sc_2O_3	C	–	9.84(1)

[a] Could not be refined due to small intensities of peaks.

[5,7,18,19]. Since there is not much variation of ionic radii across the lanthanide series, this has reflected in the prevalence of F-type phase field. Throughout the series the solubility of RE ion into CeO_2 varies between 30 and 40 mol% RE^{3+}. The same has been found true for CeO_2–Lu_2O_3 series in the present work, wherein 30 mol% Lu^{3+} was found to dissolve in CeO_2 forming F-type solid solution, The same could not be observed for Sc^{3+} (0.77 Å) since the difference in ionic radii is quite appreciable. Thus, the wider range of biphasicity and lesser solubility observed in CeO_2–$ScO_{1.5}$ series as compared to CeO_2–$LuO_{1.5}$ series can also be attributed to larger difference in ionic sizes of Ce^{4+} and Sc^{3+} as compared to that between Ce^{4+} and Lu^{3+}, which affects their miscibility behavior.

Figs. 5(a)–(c) show the back scattered images of $Ce_{0.9}Sc_{0.1}O_{1.95}$, $Ce_{0.5}Sc_{0.5}O_{1.75}$, $Ce_{0.2}Sc_{0.8}O_{1.60}$. As we move from $Ce_{0.9}Sc_{0.1}O_{1.95}$ to $Ce_{0.2}Sc_{0.8}O_{1.60}$, i.e. decrease in ceria concentration, the amount of ceria-rich phase (higher Z, F-type phase) decreases, whereas scandia-rich phase (lower Z, C-type phase) increases. This is manifested in the back scattered images of these three compositions, wherein the amount of lighter grey phase increases at the expense of heavier bright phase with increase in lutetia content. Both the bright spots (higher Z, F-type phase) and the grey spots (lower Z, C-type phase) appear to be equal in amount in $Ce_{0.5}Sc_{0.5}O_{1.75}$ since this nominal composition has both the reactants in equal amount.

Fig. 6 shows the changes in the Raman spectra with increasing concentration of $ScO_{1.5}$ in CeO_2 over the frequency range 350–550 cm^{-1}. Starting with 10 mol% $ScO_{1.5}$ till 90% of $ScO_{1.5}$ in CeO_2, the Raman spectrum shows the characteristic lines of both F and C-type structures as shown in the figure. As the doping proportion of $ScO_{1.5}$ in CeO_2 increases, only the intensity of the characteristic Raman peak of Sc_2O_3 was found to increase and that

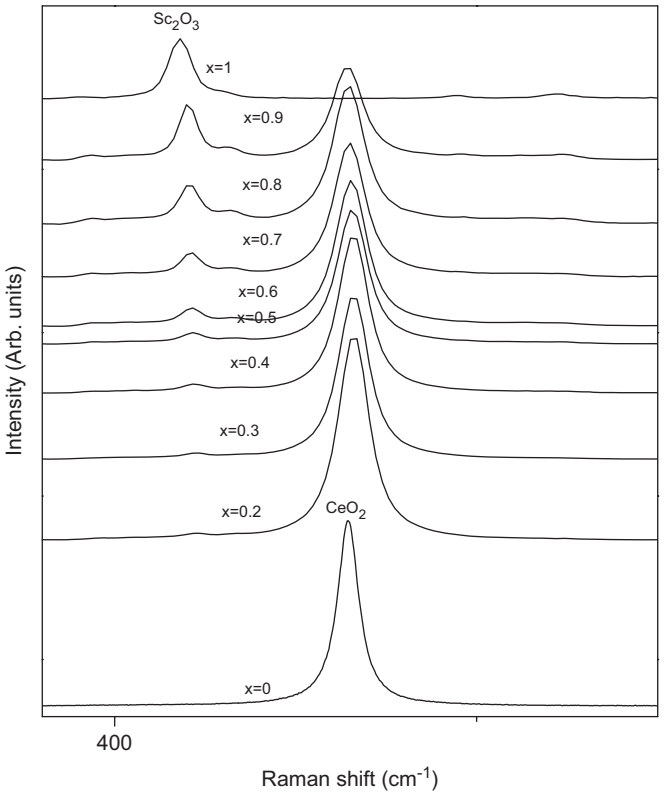

Fig. 6. Raman spectra from $Ce_{1-x}Sc_xO_{2-x/2}$ solid solution (slow-cooled) for values of x shown in the figure. Spectra have been vertically displaced for better clarity.

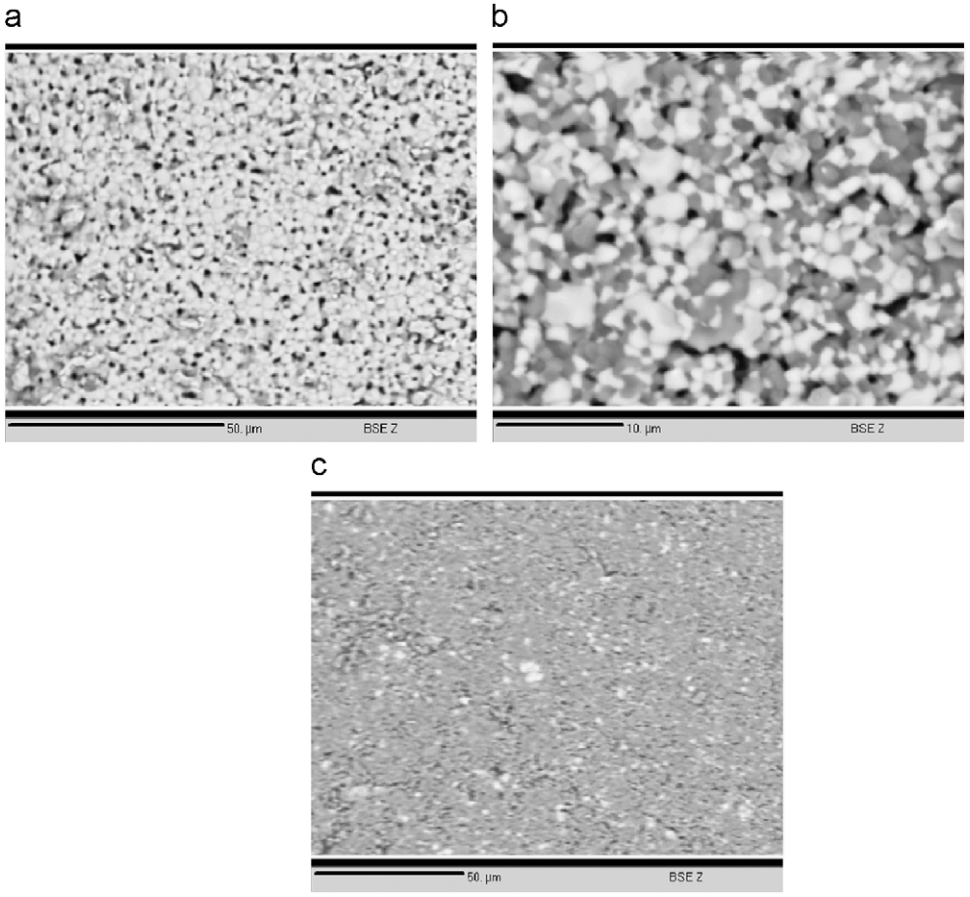

Fig. 5. Back scattered image of nominal compositions (a) $Ce_{0.9}Sc_{0.1}O_{1.95}$, (b) $Ce_{0.5}Sc_{0.5}O_{1.75}$ and (c) $Ce_{0.2}Sc_{0.8}O_{1.60}$.

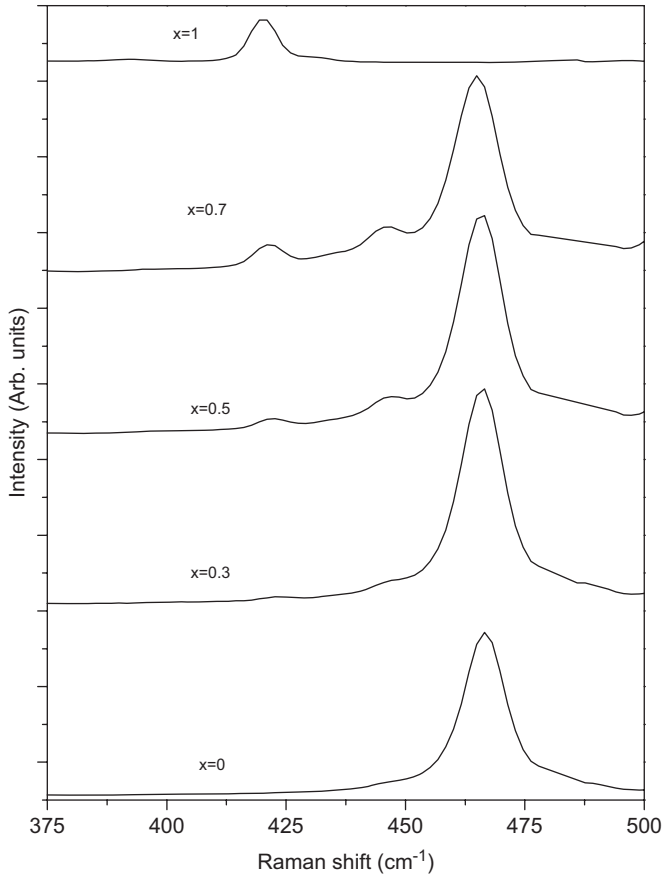

Fig. 7. Raman spectra from $Ce_{1-x}Sc_xO_{2-x/2}$ solid solution (quenched) for values of x shown in the figure. Spectra have been vertically displaced for better clarity.

of CeO_2 was found to decrease. There was no shift observed in the most intense peaks of both the phases, and we could observe the Raman signatures of both F-type and C-type structures throughout the range of CeO_2-Sc_2O_3 system. This indicates that in $Ce_{1-x}Sc_xO_{2-x/2}$; $0.1 < x < 0.9$, there exists a biphasic region consisting of both F-type and C-type structures. Also, the absence of any broad features between 200 and 600 cm^{-1} confirms the presence of any consequential doping in CeO_2 lattice. This agrees with XRD result also where similar biphasic region is observed in CeO_2–Sc_2O_3 system throughout the range. It is worthwhile to mention here that a small decrease observed in the lattice parameter of F-type solid solution was not visible in Raman spectrum in terms of shift in the intense mode of F-type phase. The decrease in lattice parameter was negligible considering the considerable difference in ionic radii of Ce^{4+} and Sc^{3+} [11], implying that a very small amount of $ScO_{1.5}$ got dissolved in CeO_2 lattice, and consequently it was not manifested in the shift of the major Raman mode at 465 cm^{-1}.

The above-mentioned studies were done on the samples slow-cooled from 1400 °C. In order to establish the changes that might occur on quenching the samples, few representative compositions from CeO_2–Sc_2O_3 and CeO_2–Lu_2O_3 series were quenched from 1450 °C and studied. All the nominal compositions that were quenched showed similar XRD patterns as the slow-cooled ones thus showing that the phase relations have not been altered by quenching the samples. In order to ascertain the XRD results, Raman spectra were recorded on these compositions. Raman spectra of few nominal compositions in CeO_2–Sc_2O_3 series are shown in Fig. 7. The results were found to be in agreement with the XRD results thus reiterating that no major changes have occurred in the samples due to quenching. This observation can be explained based on the fact that CeO_2 as well as RE_2O_3 (Sc, Lu) are very high melting solids, whereas quenching temperature used in the present work is 1450 °C, which is not expected to cause much change in the phase distribution even on quenching the samples.

4. Conclusion

The present study clearly delineates the phases present in CeO_2–Lu_2O_3 and CeO_2–Sc_2O_3 systems, and it has been demonstrated clearly using powder XRD and Raman spectroscopic techniques. CeO_2–Lu_2O_3 system shows single phasic F-type phase field up to 30 mol% $LuO_{1.5}$, and then it enters the biphasic phase field. The biphasic region consists of F-type solid solution and a pure C-type Lu_2O_3 thus reiterating the high stability of C-type Lu_2O_3, which does not accommodate any dopant into it. On the contrary CeO_2–Sc_2O_3 system was biphasic throughout, wherein the immiscibility of two reactants can be attributed to their dissimilar sizes even though slight solubility of $ScO_{1.5}$ was indicated by lattice parameter trends. The results were also aptly corroborated by back scattered images on representative nominal compositions.

References

[1] Y. Maki, M. Matsuda, T. Kudo, US Patent 3 (1971) 424.
[2] M. Yashima, H. Arashi, M. Kakihana, M. Yoshimura, J. Am. Ceram. Soc. 77 (1994) 1067.
[3] K.K.S. Pillay, Radwaste Jan. 60 (1996).
[4] W. Stoll, MRS Bull. 23 (1998) 6.
[5] K. Matsui, H. Suzuki, M. Ohgai, H. Arashi, J. Ceram. Soc. Jpn. 98 (1990) 1302.
[6] G. Adachi, N. Imanaka, Chem. Rev. 98 (1998) 1479.
[7] V. Grover, A.K. Tyagi, Mater. Res. Bull. 39 (2004) 859.
[8] A. Nakajima, A. Yoshihara, M. Ishigame, Phys. Rev. B. 50 (1994) 13297.
[9] C. Kittel, Introduction to Solid State Physics, fourth ed, Wiley, New York, 1971, p. 460.
[10] B.P. Mandal, V. Grover, M. Roy, A.K. Tyagi, J. Am. Ceram. Soc. 90 (2007) 2961.
[11] R.D. Shannon, Acta Crystallogr. A 32 (1976) 751.
[12] M. Foex, J.P. Traverse, Rev. Int. Hautes Temp. Refract. 3 (1966) 429.
[13] V.G. Keramidas, W.B. White, J. Chem. Phys. 59 (1973) 1561.
[14] W.B. White, V.G. Keramidas, Spectrochim. Acta 28A (1972) 501.
[15] C.M. Phillippi, K.S. Maazdiyasni, J. Am. Ceram. Soc. 54 (1971) 254.
[16] A. Nakajima, Y. Yoshihara, M. Ishigame, Phys. Rev. B 50 (1994) 13297.
[17] C.N. Pieczulewski, K.S. Kirkpatrick, T.O. Mason, J. Am. Ceram. Soc. 73 (1990) 2141.
[18] B.P. Mandal, V. Grover, A.K. Tyagi, Mater. Sci. Eng. A. 430 (2006) 120.
[19] B.P. Mandal, M. Roy, V. Grover, A.K. Tyagi, J. Appl. Phys. 103 (2008) 033506.